Volume 1 | Number 1 | Jan 2013 | Pages 1–100

Journal of
Materials Chemistry A

Materials for energy and sustainability
www.rsc.org/materialsA

Li⁺

ROYAL SOCIETY
OF CHEMISTRY

ROYAL SOCIETY
OF CHEMISTRY

www.rsc.org/materialsA

A-π-D-π-A based Porphyrin for solution processed small molecule bulk hetero junction solar cells

Challuri Vijay Kumar,[a] Lydia Cabau,[a] Emmanuel N. Koukaras,[b,c], Abhishek Sharma[d],
Ganesh D. Sharma*[e] and Emilio Palomares*[a,f]

[a]Institute of Chemical Research of Catalonia (ICIQ), Avda. Països Catalans 16, E-43007
Tarragona, Spain

[b]Institute of Chemical Engineering Sciences, Foundation for Research & Technology, Hellas,
Stadiou Str. Platani, Patras, 26504, Greece

[c]Molecular Engineering Laboratory, Department of Physics, University of Patras, Patras,
26500 GR, Greece

[d]Department of Electronics and Communication, LNMIIT, Jamdoli, Jaipur, India

[e]R & D Center for Engineering and Science, JEC group of Colleges, Jaipur Engineering
College, Kukas, Jaipur 303101, India. E-mail: gdsharma273@gmail.com, and
sharmagd_in@yahoo.com

[f]Catalan Institution for Research and Advance Studies (ICREA), Avda. Lluis Companys 23,
E-08010 Barcelona, Spain. E-mail: epalomares@iciq.es

In this article, we have designed and synthesized a porphyrin with the following molecular architecture A–π-D–π-A in which ethyl rhodanine end capping groups were linked to core porphyrin donor via octyl thiophenes -ethynylene π bridge denoted as **VC117** and used it as electron donor along with the ([6,6]-phenyl C_{71} butyric acid methyl ester) (PC$_{71}$BM) as electron acceptor for the fabrication of solution processed organic solar cells. The solution processed BHJ organic solar cell with an optimized weight ratio of 1:1 **VC117**:PC$_{71}$BM in THF (tetrahydrofuran) showed an overall power conversion efficiency (PCE) of 2.95 % with short circuit current J_{sc}= 8.34 mA/cm^2, open circuit voltage V_{oc}= 0.82 V and fill factor FF =0.43. Nonetheless, when the active layer of the solar cell was processed from a mixture of 4% v/v of pyridine in THF solvent, it achieved a PCE value of 4.46 % and further improved up to 5.50 % followed by the thermal annealing. This is ascribed to the enhancement of both the J_{sc} and the FF values. The higher value of J_{sc} is explained by the increased absorption profile of the blend, the higher incident photon to current efficiency (IPCE) response and the better crystallinity of the active layer when processed with solvent additive and thermal annealing while the enhancement of FF is due to the better charge transport capability and the charge collection efficiency in the later device.

Key Words: A–π-D–π-A porphyrin, Bulk heterojunction small molecule solar cells, solvent additive, thermal annealing, power conversion efficiency

* Corresponding authors E-mail: gdsharma273@gmail.com, sharmagd_in@yahoo.com (G. D. Sharma), and epalomares@iciq.es (Emilio Palomares)

Introduction

Bulk heterojunction organic solar cells, consist of a blend of conjugated polymer donor and fullerene derivative as electron acceptor, and convert the energy of sunlight directly into electrical energy. They have attracted more and more ever increasing interest due to their low cost, roll to roll manufacturing, environmentally friendly processing, lightweight properties and mechanical flexibility [1]. Bulk heterojunction organic solar cells (BHJ-OSCs) using donor-acceptor (D-A) copolymers as electron donor and $PC_{71}BM$ have showed a power conversion efficiency (PCE) over 10 % in single BHJ solar cells and 10.6 % [2] in tandem solar cells [3]. This progress is a direct result of the development of different materials including electron donor [4] and electron acceptor materials [5], along with the innovations and optimizations in device processing and engineering [6]. In spite of these advances in the polymer based BHJ solar cells, there are two main disadvantages of the conjugated polymers i.e. the purity of materials and variations in the molecular weights and this makes these materials of photovoltaic properties difficult to reproduce [7] in a systematic manner. In recent years, solution processed small molecules solar cells have been emerging as a competitive alternative to that of copolymers due to the their advantages, that include versatile chemical structures, and easier to energy level control, mobility tuning and less batch to batch variations [8], and for which PCE in the range of 8-10 % have been reported for these solar cells [9].

For a solution processed BHJ small molecule solar cell, the donor small molecule plays a very important role in absorbing incident light on the device, they should posses a strong and wide absorption profile that closely matches with the solar spectrum. In this regards, porphyrin derivatives, owing to their very well established potential as light harvesting antennae for efficient energy and electron transfer processes in biological systems, appears to be very attractive as donors in organic solar cells [10]. These materials display an absorption spectra with intense Soret band at 400-450 nm and moderate Q bands at 500 -700 nm, due to their π-conjugated macrocyclic frame work. Moreover, their electronic, spectroscopic and physical properties can be appropriately tuned by synthetically modifying the substituents of the macrocyclic ring and/or the metal into the central cavity [11]. Porphyrin derivatives have been successfully employed as sensitizers for dye sensitized solar cells [12] and some of them have showed PCE of over than 12-13% [13]. But, the use of porphyrin as donor in solution processed BHJ organic solar cells is limited due to the

difficulty of their solubility in common organic solvents which is one of the most important requirements for these types of devices. However, the appropriate selection of peripheral substituents can increase the solubility of porphyrins. Matsuo et al. have reported the synthesis of soluble porphyrins consisting of tetraethyl porphyrin cores with two aromatic and two aliphatic groups at *trans* positions and used them as donor along with $PC_{60}BM$ as the electron acceptor for solution processed BHJ organic solar cells and achieved a PCE of 2.5% [14]. With the above consideration in mind, many porphyrin derivatives have been synthesized by different research groups and used as donor for solution processed BHJ solar cells and moderate PCE has been reported [15]. Peng et al. employed a porphyrin molecule with less bulky substituents at the periphery as donor material along with $PC_{61}BM$ as the acceptor for solution processed organic solar cells and achieved a PCE up to 7.23% [16a]. Recently, Gao et al have achieved a PCE of 8.08 % for solution processed BHJ solar cell with porphyrin having low bandgap of 1.37 eV [16b].

For the conjugated small molecules, with acceptor –donor –acceptor structures, many promising end groups have been reported, these include dicyanovinyl (CN) [17], alkyl cyanoacetate [18] and 3-ethylrodanine [19]. Recently, Liu et al have designed a small molecule with 3-octylrodanine as the electron-with-drawing end-group and BDT-T as the core unit and reported a PCE of 8.02 % for solution processed BHJ organic solar cell, using this small molecule as donor and $PC_{71}BM$ as electron acceptor [9e]. An A-π-D-π-A molecular structure with a conjugated donor backbone and an electron withdrawing terminals has several advantages for use in BHJ organic solar cells: (i) high mobility with planar structure and efficient π-π interactions, (ii) a low bandgap resulting from intramolecular charge transfer and (iii) good film quality owing to a long conjugated backbone with dispersed alkyl chains similar to polymers. Recently, we have designed an A–π-D–π-A porphyrin small molecule in which the di-cyanovinyl substituted thiophene (A) was linked by ethynylene to the porphyrin core with high solubility and used it as electron donor along with $PC_{71}BM$ as electron acceptor for solution processed solar cells and achieved a PCE of 5.34 % [20].

In continuation to our research work in the field of small molecules for solution processed BHJ solar cells, we report the design and synthesis of an A–π-D–π-A porphyrin small molecule in which ethyl rhodanine end capping groups were linked to core porphyrin donor via octyl thiophenes -ethynylene π bridge. An ethynylene link makes the octyl thiophenes moiety coplanar to the porphyrin core thus promoting an extensive π-conjugated

region. We have used this porphyrin small molecule as a donor along with the $PC_{71}BM$ as the acceptor for the fabrication of BHJ solution processed organic solar cells. Moreover, we have shown that the nanomorphology of the **VC117**:$PC_{71}BM$ active layer could be improved by the solvent additive pyridine with an enhanced balanced charge transport and the PCE of up to 5.56 % has been achieved for the optimized BHJ organic solar cell. The enhancement in the PCE is mainly to the improved values of J_{sc} and FF, attributed to the combination of light harvesting efficiency, exciton dissociation efficiency and charge transport ability, due to the improved nanoscale morphology and interpenetrating pathways, induced by the solvent additives.

Experimental details

General

Unless stated otherwise, all reagents were purchased from commercial sources and used without further purification. Dichloromethane, Pyrrole, Pyridine, Dichloroethane, Ethanol and THF were distilled before use. Ethyl rhodanine, DDQ, $_4$, $Pd_2(dba)_3$, $AsPh_3$, N-bromosuccinimide (NBS), were purchased from Sigma-Aldrich. Dry THF and toluene were obtained by passing them through an activated alumina column on a PureSolv^{TM} solvent purification system (Innovative Technologies, Inc., MA). Flash column chromatography was carried out using Silica gel 60, 40-63 μm (Panreac Química SLU) as the stationary phase. Size exclusion chromatography was carried out in a large elution column (1000mm x 38 mm) with Biobead SX3 (Bio-Rad Laboratories, Inc.) as the stationary phase. The eluent was passed through the column under gravity. 5-bromo-3,3-dioctyl-2,2:5,2-terthiophene-2-carbaldehyde (Br_3TCHO) [21] and octyloxy diacetylene porphyrin [22] was synthesized as per the earlier reported procedure.

Experimental

UV-vis absorption spectra were measured in a 1 cm path-length quartz cell using a Shimadzu model 1700 spectrophotometer. Steady state fluorescence spectra were recorded using a Spex model Fluoromax-3 spectrofluorometer using a 1 cm quartz cell. All ^1H and ^{13}C NMR spectra were recorded on a Bruker AV 300 and AV 500 instruments, respectively, at a constant temperature of 300 K, unless otherwise stated. ^1H spectra were referenced to tertramethylsilane. ESI mass spectra were recorded on a Water Quattro micro (Water Inc, USA). Cyclic voltammetric experiments were carried out with a PC-controlled CH instruments model CHI620C electrochemical analyzer. Flash column chromatography was carried out using Silica gel 60, 40-63 μm (Panreac Química SLU) as the stationary phase.

Size exclusion chromatography was carried out in a large elution column (1000mm x 38 mm) with Biobead SX3 (Bio-Rad Laboratories, Inc.) as the stationary phase. The eluent was passed through the column under gravity.

Synthesis of 3: 1 (300 mg, 0.519 mmol) was dissolved in a solution of dry chloroform (30 mL) and two drops of piperdine and 3-ethyrhodanine **(2)** (417 mg, 2.59 mmol) was added and the resulting solution was heated to reflux and stirred for 24 hours under argon. The reaction mixture was cool to room temperature, and then water was added. The crude product was extracted into $CHCl_3$, and the organic layer was dried over Na_2SO_4. The solvent was removed under reduced pressure and the crude product was purified by column chromatography on silica gel using CH_2Cl_2 and hexane (1:1) as eluent to afford the desired product. ^{1}H NMR (Figure S1, supporting information) (300 MHz, Chloroform-d) δ 7.75 (s, 1H), 7.17 (s, 1H), 7.16 (d, 1H, J=4.0Hz), 7.02 (1H, d, J=3.6Hz), 6.88(1H, s), 4.16 (2H, q), 2.75 (4H, m),1.61(20H,m), 0.83(9H,m).^{13}C NMR (75 MHz, $CDCl_3$) (Figure S2, supporting information) δ.191.42, 166.73, 140.64,140.22,138.51,136.51,136.03, 134.74, 134.48, 132.22, 130.68, 126.58, 126.13, 124.19, 120.13, 110.58, 39.25, 31.28, 29.92, 29.71, 29.07, 28.87, 28.80, 28.74, 28.67, 28.614, 22.01, 13.44, 11.64. MS (MALDI-TOF) (Figure S3, supporting information): calcd for [M]+, 721.1239

Synthesis of VC117:

In a dry Schlenck tube **4** [22] (150 mg, 0.138 mmol) **3** (249 mg, 0.34mmol) were dissolved in a mixture of dry THF (20 mL) and NEt_3 (5 mL) and the solution was degassed with di nitrogen for 10 min; $Pd_2(dba)_3$ (75 mg, 0.08 m mol) and $AsPh_3$ (168 mg, 0.552 m mol) were added to the mixture. The solution was refluxed for 12 h under nitrogen atmosphere. The solvent was removed under reduced pressure and the crude product was purified by silica gel column chromatography using chloroform and hexane (1:1) as eluent and subsequent size exclusion chromatography using THF as eluent to obtain a purple solid.^{1}H-NMR (Figure S4, supporting information) (300MHz,THF-d8) $δ_H$ 9.48(4H, d), 8.75(4H, d), 7.87(s, 2H), 7.69(t, 2H), 7.59(d, 2H), 7.47(s, 2H), 7.41(d, 2H), 7.36(d, 2H), 7.02(d, 4H), 4.16(m, 4H), 3.66(m, 4H), 2.96(m, 8H), 1.30(m, 60H), 0.86(m, 44H), 0.64(m, 30H).^{13}C NMR (75 MHz, THF-d8) (Figure S5, supporting information) δ.191.42, 166.53, 160.03, 150.97, 150.56, 141.05, 140.14, 140.58, 138.59, 137.73, 137.12, 135.62, 135.02, 134.45, 131.52, 131.16, 129.73, 129.59, 127.91, 127.59, 126.81, 124.89, 123.31, 120.99, 120.60, 115.49, 104.57, 99.47, 98.68, 88.05, 39.52, 37.18, 34.14, 32.79, 31.92, 31.94, 31.55, 30.52, 30.26, 30.08, 29.80, 29.70, 29.60, 29.52, 29.43 29.29, 28.87, 28.79, 25.41, 22.61,

22.31, 13.51,13.37,11.36.MS (MALDI-TOF) (Figure S6, supporting information): calcd for [M]+, 2370.9. . Anal. Calcd. For $C_{136}H_{170}N_6O_6S_{10}Zn$ C, 68.90; H, 7.23; N, 3.54; O, 4.05; S, 13.52 Found C, 71.46; H,8.16; N,2.97; S,10.57.

We would like to notice that VC117 was purified by consecutive flash chromatography , size exclusion chromatography and also HPLC. However, although this combination of techniques was effective to remove almost all major impurities, a by-product was still present (as can be seen at the 1H-NMR). It is estimated that the final product has a degree of purity higher than 95%. The implications on the device solar cell performance are detailed below.

Device fabrication and characterization

The BHJ organic solar cells were fabricated using the glass/ITO/PEDOT:PSS/**VC117**:$PC_{71}BM$ /Al device architecture. The indium tin oxide (ITO) patterned substrates were cleaned by ultrasonic treatment in aqueous detergent, deionized water, isopropyl alcohol, and acetone sequentially, and finally dried under ambient conditions. The anode consisted of glass substrates percolated with ITO, modified by spin coating with a PEDOT:PSS layer (60 nm) as hole transport and heated for 10 min at 100℃. Mixtures of **VC117** with $PC_{71}BM$ with weight ratios of 1:0.5, 1:1, and 1:1.5 in tetrahydrofuran THF were prepared and then spin-cast onto the PEDOT:PSS layer and dried overnight at ambient atmosphere. For the **VC117**:PC_{71} BM blend processed from 1, 2, 3, 4% and 5 % v/v of pyridine in THF solvent mixture only the 1:1 weight ratio mixture was used. The total concentration of mixture was 10 mg/ML for each active layer. The approximate thickness of the active layers was 90 nm. We have prepared the **VC117**:$PC_{71}BM$ active layer processed under different conditions: **VC117**:$PC_{71}BM$ (processed with THF) for device A, **VC117**:$PC_{71}BM$ (pyridine/THF cast) for device B and **VC117**:$PC_{71}BM$ (pyridine/THF cast and subsequent thermal annealing at 110° C for 10 min) for device C. For the thermal annealing, the active layer cast from pyridine/THF was placed on the hot plate at 110° C for 10 min. Finally, the aluminum (Al) top electrode was thermally deposited on the active layer at a vacuum of 10^{-5} Torr through a shadow mask of area of 0.20 mm^2. All devices were fabricated and tested in ambient atmosphere without encapsulation. The hole-only and electron-only devices with ITO /PEDOT:PSS/**VC117**:$PC_{71}BM$/Au and ITO/Al/**VC117**:$PC_{71}BM$/Al architectures were also fabricated in an analogous way, in order to measure the hole and electron mobility, respectively. The current-voltage (J-V) characteristics of the BHJ organic solar cells were measured using a computer controlled

Keithley 238 source meter in dark and under simulated AM 1.5G illumination of 100 mW/cm^2. A xenon light source coupled with optical filter was used to give the stimulated irradiance at the surface of the devices. The incident photon to current efficiency (IPCE) of the devices was measured illuminating the device through the light source and monochromator and the resulting current was measured using a Keithley electrometer under short circuit condition.

XRD measurements were recorded on a Bruker D8 Advanced model diffractometer with Cu Kα radiation (λ = 1.542 Å) at a generator voltage of 40 kV.

Results and discussion

Synthesis and characterization

The synthetic route of the porphyrin small molecule **VC117** in the Scheme 1 and Scheme The targeted molecule based on the A-π-D-π-A architecture is scheme 2. The **VC117** porphyrin molecule was synthesised via sonagashira coupling reaction bromo terthiohene rhodanine (3) with diacetylene porphyrin in the presence of dry THF,NEt$_3$,Pd$_2$(dba)$_3$ and AsPh$_3$.The intermediate (3) was synthesised via Knoevenagel condensation of ethylrodanine with bromo terthiophene aldehyde   in the presence of pippredine. The important intermediates and the targeted porphyrin small molecule **VC117** was well characterized by ^{1}H-NMR, ^{13}CNMR, and MALDI TOF mass spectroscopy. **VC117** was purified by consecutive flash chromatography, size exclusion chromatography. This combination of technique was found effective to purify the molecule to acceptable levels for device fabrication. The central atom porphyrin unit was functionalized with octyl terthiohene π bridge and acceptor ethyl rhodanine as terminal unit. The symmetrical structure of the porphyrin small molecule is expected to enhance the π-π stacking interactions which could be beneficial for high mobility. The terminal unit ethyl rhodanine acceptor adjusting the HOMO-LUMO energy levels of the porphyrin small molecule. The introduction of the long alkyl chain to the porphyrin and terthiophene increases the solubility and soluble in common organic solvents.

Photophysical and electrochemical properties

The normalized optical absorption spectra of **VC117** in dilute THF solution and thin film cast from the THF solvent is shown in Figure 1 and complied is table 1. The **VC117** exhibits a strong Soret band in the wavelength range 400 -550 nm with an absorption peak at 467 nm and a moderate Q band in the wavelength range 620 –720 nm with a peak around 682 nm and is the typical characteristics of ethynyl linked based porphyrins [23]. The Soret band

of **VC117** is broadened and also redshift and the Q band is also redshift and intensify, as compared to other porphyrins may be attributed to intramolecular charge transfer (ICT) between the donor and acceptor units. These spectral changes indicate an effective π-elongation through the porphyrin core, octyl thiophenes -ethynylene π bridge and ethyl rhodanine and better conjugation for **VC117** [24]. As compared to absorption spectrum in solution, the thin film absorption spectra showed slight red shift and broadening in both Soret and Q bands. A red shift of about 18 nm in Q band attributed to strong intermolecular interaction in solid state. The optical bandgap of **VC117** is estimated from the onset of the absorption spectrum in thin film and is about 1.62 eV. This porphyrin molecule exhibits a wide absorption from 400 to 760 nm with high absorption coefficients owing to the efficient conjugation in the backbone structure and intramolecular charge transfer between the terminal acceptor units and core donor through the π-linker.

Cyclic voltammetry (CV) was used to estimate the highest occupied molecular orbital (HOMO) of **VC117**. The potential were internally calibrated using the ferrocene/ferrocenium (Fc/Fc$^+$) of the redox couple (4.8 eV below vacuum level). The HOMO which is -5.13 eV for **VC117** was estimated from the onset oxidation and reduction potential. The LUMO energy level was determined using E_{LUMO}= EHOMO-E_{o-o}. E_{o-o} is the energy between the energy transition between the lowest vibrational ground state and the lowest vibrational excited state and calculated from the intersection of absorption and emission spectra of small molecules in solution (Figure S7, supporting information). The calculated LUMO energy levels of **VC117** is -3.36 eV is above the LUMO energy level of PC$_{71}$BM (-4.1 eV) that act as electron acceptor, which generates a large driving force for the transfer and separation of photogenerated charge carriers in the D-A interface.

Theoretical Calculations

We have additionally performed a theoretical study on the **VC117** molecular structures within the framework of density functional theory (DFT) and time-dependent density functional theory (TD-DFT).

The initial geometry optimization calculations were performed employing the gradient corrected functional PBE [25] of Perdew, Burke and Ernzerhof. The def-SVP basis set [26] was used for all of the calculations. At this stage of the calculations, to increase the computational efficiency (without loss in accuracy), the resolution of the identity method [27] was used for the treatment of the two-electron integrals. Subsequent geometry optimization were further performed using the hybrid exchange–correlation functional B3LYP [28] as well as Truhlar's meta-hybrid exchange–correlation functional M06 [29], and the same basis set.

Tight convergence criteria were placed for the SCF energy (up to 10^{-7} Eh) and the one-electron density (rms of the density matrix up to 10^{-8}) as well as for the norm of the Cartesian gradient (residual forces both average and maximum smaller than 1.5×10^{-5} a.u.) and residual displacements (both average and maximum smaller than 6×10^{-5} a.u.). Solvent effects were included for the THF using the integral equation formalism variant of the Polarizable Continuum Model (IEFPCM), as implemented in the Gaussian package [30]. TD-DFT excited state calculations were performed to calculate the optical gap of **VC117** using the same functionals and basis set on the corresponding ground state structures. The UV/Vis spectra were calculated using the B3LYP and M06 functionals. The first round of geometry optimization was performed using the Turbomole package [31]. All of the follow up calculations were performed using the Gaussian package [30].

The first round of calculations was geometry optimizations using initial geometries with various orientations of the moieties that compile the **VC117** structure. To increase the computational efficiency of the next rounds, for which the hybrid B3LYP and meta-hybrid M06 functionals were used, the alkyl groups were truncated to ethyl groups. Vibrational analysis on the optimized structure **VC117** did not reveal any vibrational modes with imaginary eigenfrequencies, i.e. the final optimized structures are true local (if not global) minimum. The main inner body of the structures is highly planar, this includes the porphyrin structure up to (and including) the first thiophene moiety. The two outer rings are coplanar which is mainly as the result of the unsaturated linking carbon. The thiophene group that links the outer and inner structure forms dihedral angles ~17°–22° and ~28°–32° with the inner and outer structure, respectively, depending on the functional and the presence of solvent. The planes of the phenyl groups linked to the porphyrin form almost normal dihedral angles to the main body plane. We have calculated the HOMO and LUMO energy levels and the optical gaps, defined here as the energetically lowest allowed vertical electronic excitation, employing the PBE, M06, and B3LYP functionals. In Table 2, in addition to the frontier orbitals' energy levels, we also provide the optical gap the main contributions to the first excitation as well as the wavelength of the first excitation and of the excitations with the largest oscillator strengths.

In addition to the B3LYP functional we have also performed our calculations employing the M06 functional. The M06 meta-hybrid functional was chosen since it provides leveled performance over transition types [32, 13a]. We provide results using all three functionals, which can additionally be used for comparison with the literature. The HOMO–LUMO (HL) gap calculated using the hybrid B3LYP functional is slightly smaller than that

using the meta-hybrid M06 functional and however, the calculated optical gaps are practically the same for both functionals. In Table 2 we also provide the character of the first allowed excitations only for contributions larger than 4%. The first excitation, as calculated by each of the functionals, clearly exhibits a strong single-configuration character, with only marginal secondary contributions.

In Figure 2 we have plotted the isosurfaces (isovalue=0.02) of the HOMO and LUMO, as well as the next nearest frontier orbitals of **VC117** which are involved in transitions with strong contributions to the first excitation. The HOMO extends over all of the main body of the structures that is planar and includes the first (inner) thiophene and the linking thiophene moieties. The LUMO is delocalized mainly on the inner part of the structures, but also extends over the all of the ring groups, however with smaller contributions. We also show the HOMO–1, HOMO–1, and LUMO+2, LUMO+3 isosurfaces since transitions between them contribute to the first excitations, as shown in Table 2. The delocalizations exhibited from these orbitals vary, with the HOMO–2 and LUMO+3 mainly on the porphyrin, and the HOMO–1 and LUMO+2 over the thiophene chain or the terminating thiophenethiazolidin4one (**TPTAO**) ring groups. To quantify the contributions of the moieties to the frontier orbitals we have calculated the total and partial density of states (PDOS). The PDOS for **VC117** is shown in Figure 3. We partition the structure into the diPhenylPorphyrine, **dPPorph**, central structure, the first thiophene group bonded to the porphyrin, **TPa**, the thiophene that links the inner and outer structure, **TPL**, the TPTAO outer ring, and all the alkyl groups collectively. The HOMO is dominated by contributions from the **dPPorph** and **TPA** groups by 50% and 33.6% respectively, as well as a significant contribution of 9.9% from the linking thiophene **TPL**. A similar pattern is found for the LUMO to which the dPPorph and TPA contribute 52.3% and 21.3% respectively, however in this case with significant contributions from **TPTAO** at 18.7% and from **TPL** at 7.4%. It is thus not expected transitions from HOMO to LUMO to result in significant charge transfer. The near frontier orbitals exhibit different character, specifically, the contributions from **TPA**, **TPTAO**, **dPPorph** and **TPL** are 30.5% (0.0%), 33.1% (0.0%), 6.4% (99.9%), and 28.1% (0.0%) for HOMO–1 (HOMO–2). Similarly, the corresponding contributions to LUMO+2 (LUMO+3) are 5.2% (0.0%), 69.8% (0.0%), 19.1% (99.8%), and 5.6% (0.0%). These are in agreement with our earlier observations on the orbital delocalizations. From the pattern that emerges any charge transfer from HOMO–1 to LUMO+3 transitions is compensated from HOMO to LUMO+2. On the other hand, no charge transfer is expected from a HOMO–2 to LUMO+3 transitions. Overall the first excitation does not result in

charge transfer. The first significant contributions (5.1%) from the aliphatic groups are noted at lower energies, about –6.7 eV which corresponds to the HOMO–10 level.

In Figure 4 we show the UV/Visual absorption spectra of the **VC117** structure calculated at the TD-DFT/M06 level of theory, both accounting for solvent effects for CF and in gas phase. The spectra have been produced by convoluting Gaussian functions with HWHM = 0.18 eV centered at the excitation wavenumbers. In Figure SI-1 (see Supporting Information) we also provide the corresponding spectra calculated using the B3LYP functional, which only slightly overestimates the wavelengths and retains all the main characteristics with that using M06 and the experimental spectra. The absorption spectra of the two structures exhibit two main bands that are located on the high and low wavelength regions. The low wavelength region exhibits a finer structure which manifests as a side bump at lower wavelengths. The first band is centered at 724 nm and the second at 497 nm. The wavelengths of the excitations with the largest oscillator strengths within these bands are given in Table 2.

Photovoltaic properties

The photovoltaic performance of the organic solar cell that uses the BHJ active layer with a mixture of donor and acceptor materials is significantly influenced by the relative concentrations of these components used for the preparation of the active layer as there should a balance between the absorbance of incident photons and subsequent charge transport process within the active layer. When the concentration of the acceptor material is low, the electron transporting ability will be limited while with the higher amount of acceptor concentration, the absorbance and hole transport ability in the active layer will be decreased. In our system, the optimum device performance was observed in a blend of 1:1 weight ratio of the mixture **VC117** and $PC_{71}BM$ in THF, after testing the devices with a series of three different weight ratios (1:0.5, 1:1 and 1:1.5). From the normalized absorption spectrum of this blend **VC117**:$PC_{71}BM$ (1:1) (Figure 5) that shows the combination of both **VC117** and $PC_{71}BM$ absorption characteristics, it becomes obvious that both moieties participate in light absorption and thus photocurrent generation.

The current –voltage characteristics of the device based on optimized **VC117**:$PC_{71}BM$ (1:1) active layer processed from THF solvent (device A), under stimulated solar illumination (100 mW/cm^2) is shown in Figure 6a and photovoltaic parameters are complied in Table 3. The device showed an overall PCE of 2.95 % with Jsc =8.38 mA/cm^2, Voc= 0.82 V and FF=0.43. The V_{oc} of the device based on **VC117** is respectable, however it is lower than that of the porphyrin dye VC62 [20], which may be related to the higher value

of the HOMO energy level of **VC117** (-5.13 eV) as compared to VC62 (-5.44 eV). The incident photon to current conversion efficiency (IPCE) of the device based on **VC117**:PC$_{71}$BM (1:1, THF) is shown in Figure 6b and it is found that this spectrum is closely related to absorption spectrum of **VC117**:PC$_{71}$BM blend (as shown in Figure 5), indicating that both **VC117** and PC$_{71}$BM contribute to photocurrent generation.

Nevertheless, the overall PCE value of the organic solar cell based on **VC117**:PC$_{71}$BM active layer processed from THF is smaller than that reported in the literature when other small molecules are used as donors. The inferior performance can also be attributed to the fact, as mentioned at the Experimental Section, that the **VC117** has purity above 95% only. A seminal paper by Heeger and co-workers in 2011 describes how " small amounts of impurity, even one part in one thousand" can lead to noticeable decrease in solar cell efficiency [33]. Nonetheless, the V_{oc} of the present device is excellent (V_{oc} = 0.82 V) and the lower PCE value is mainly due to the low values of both J_{sc} and FF. These two parameters are directly related to the light harvesting efficiency of active layer and the resulting charge generation as well as to the charge transport and collection to the respective electrodes, processes that depend on the film morphology. A well defined nanomorphology and phase separation between donor and acceptor components in the active layer within the range of exciton diffusion length is necessary for efficient exciton dissociation and charge transport [34]. It is reported that controlling the morphology of active layer, induced by the appropriate treatment methodologies, i.e., thermal annealing [35], solvent annealing [36] and solvent additives [37], the photovoltaic performance of BHJ organic solar cells based on either conjugated polymers or small molecules can be significantly improved. Particularly, the choice of solvent plays a very important role and influences greatly the overall PCE of organic solar cell based on BHJ active layer. Recently, the solvent additive method was used to improve the performance of BHJ organic solar cells using porphyrins as electron donors and PC$_{71}$BM as electron acceptor with remarkable results [15c, 16]. Aiming to improve the overall PCE value of our device based on the optimized **VC117**:PC$_{71}$BM active layer, we have employed the solvent additive treatment method using a small amount of pyridine as solvent additive (device B), as it is known to be more effective than other solvent additives for porphyrin based BHJ solar cells. We have added different amounts of pyridine (1, 2, 3, 4 and 5 % v) and found the 4 v% is the optimized concentration (device B). In order to improve the PCE of the device, we further thermally annealed the solvent additive cast **VC117**:PC$_{71}$BM film at 110° C for 10 min (device C). The J-V characteristics and IPCE

spectra of the device B and C are shown in Figure 6a and 6b, respectively. The device B and C showed a PCE of 4.46 % (J_{sc}= 10.22 mA/cm^2, V_{oc} =0.78 V and FF= 0.56) and 5.50 (J_{sc} =11.67 mA/cm^2, V_{oc} =0.76 V and FF=0.62), respectively. The improvement in the PCE is mainly due to the enhancement in both J_{sc} and FF. The improvement in the value of J_{sc} for device B and C is consistent with the IPCE spectra of the devices, i.e. the values of IPCE are higher for B and C as compared to device A throughout the whole wavelength range of measurements. The J_{sc} values estimated from the integration of IPCE spectra of corresponding devices are 8.24 mA/cm^2, 10.13 mA/cm^2 and 11.54 mA/cm^2, for device A, B and C, respectively. These values are consistent with the values estimated from J-V characteristics of the corresponding devices. The improvement in the PCE after additional treatment i.e. solvent additive and subsequent thermal annealing has been mainly attributed to the significant enhancement in both J_{sc} and FF and may be originated from the enhanced absorption, better morphology of the active layer and higher and more balanced charge carrier mobilities.

To get information about the improved performance of the device B and C, we have measured the optical absorption spectra of the blends used for device A, B and C, i.e. active layer cast from THF, pyridine/THF and pyridine/THF (thermally annealed) and is shown in Figure 5. As shown in figure 5, the absorption intensity of the pyridine /THF cast blend film is enhanced and ICT band corresponds to **VC117** is redshifted as compared to THF cast blend film which is related to the enhanced π-π stacking between the molecule backbones [38]. For the film with further thermal annealing, the absorption intensity was further improved. These results indicates that the solvent additive and subsequent thermal annealing improved the light harvesting ability of the active layer and one of the reasons for the enhancement in J_{sc} of the device B and C.

The difference in PCE of the solar cell, when the active layer was spin cast from pyridine/THF solution, may be the difference in exciton dissociation efficiency, after the exciton generation. Photoluminescence (PL) quenching provides direct evidence for the exciton dissociation, which influences the J_{sc} and is used as a measure of photoinduced charge transfer between donor and acceptor interface present in the active layer. PL was measured to investigate the exciton dissociation efficiency. Figure 7 shows the PL spectra of spin coated **VC117** (THF cast) and **VC117:**PC$_{71}$BM (1:1) (THF and pyridine/THF cast) blend films. As can be seen from this figure that the pristine **VC117** exhibits PL emission with a peak around 716 nm. Blending **VC117** with PC$_{71}$BM, the PL peak is quenched. The

degree of quenching increases with the addition of pyridine. This effective PL quenching suggest that the exciton separation was more efficient in the active layer cast from pyridine/THF as compared to that for THF cast active layer. The more effective quenching in the pyridine/THF cast film than in THF cast film implies two possibilities: (i) better exciton dissociation in the pyridine /THF cast film, (ii) a larger interfacial area between the **VC117** and $PC_{71}BM$ through the optimal nanoscale phase separation. The former could be ruled out, because this is affected mainly by the energy difference between the HOMO of the donor and LUMO of the acceptor used in the blend. The second mechanism is mainly responsible for the effective PL quenching as confirmed from the active layer film morphology studies. Thus the optimized phase separation and crystallinity of the active layer are important factor for efficient exciton dissociation. The morphology and quenching of PL intensity revealed that the active layer processed with pyridine/THF exhibits more favorable features for higher J_{sc}.

The morphology of the thin film was characterized by transmission electron microscopy (TEM) and shown in Figure 8 for the active layers employed for device A, B and C. The thin film processed with THF form large phase separated domain of sizes 90-100 nm which is significantly larger than the exciton diffusion length. This large scale phase separation affects the exciton dissociation into free charge carrier and their transportation and leads to the reduction in J_{sc} and FF. The film cast from the pyridine/THF had smaller domain sizes and were further reduced up to 20-25 nm with additional thermal annealing. The better morphology and optimized interpenetrating networks of blend active layer films with TA and SATA treatment leads to increased donor-acceptor interfacial area and hole mobility, which may increase the exciton dissociation and charge transport efficiency and reduces the charge carrier recombination, thus resulting in higher J_{sc} and FF [39].

The crystallinity of the active layer also plays an important role in the charge transport and collection, thereby increasing the overall PCE of the organic solar cell. To obtain information about the change in the crystallinity of the **VC117**:$PC_{71}BM$ film with the addition of pyridine in the host solvent, prior to the spin casting, we have recorded the X-ray diffraction (XRD) pattern of the spin cast thin film processed with and without pyridine additive. In addition, we have also recorded the XRD patterns of pristine **VC117** thin film cast from THF and pyridine/THF solvents, for comparison (Supporting information Figure). The pristine **VC117** cast from THF as well as from pyridine/THF shows strong diffraction peak at 2θ=7.22°, but the intensity of the later is stronger than the one of the former, indicating that the crystallinity of the film is increased with the addition of pyridine additive.

The blend **VC117**:PC$_{71}$BM cast from THF (black color Figure 9a) also shows a diffraction peak at around 2θ=7.22°, corresponding to **VC117** unit but its intensity becomes weak, suggesting an effective mixing of PC$_{71}$BM and **VC117.** However, this diffraction peak becomes more intense in the corresponding blend cast from pyridine/THF solvent, while its width at half maximum height is decreased. These results indicate that the blend film cast from the THF solvent has low crystallinity, while in the case of blend film cast from pyridine/THF solvent, the crystallinity and π conjugation of **VC117** in the blend increases. The intensity further increased with additional thermal annealing. This is probably due to the difference in the boiling point of THF and pyridine that makes the spin coated film to dry slowly, assisting in the formation of a better self ordered structure of the blend. The increase in the crystallinity leads to an enhancement in the light absorption property of the active layer and higher hole mobility in the blend film, leading to the increase in J$_{sc}$, FF and PCE of the organic solar cell.

The charge carrier mobility in the BHJ active layer is critical in the BHJ organic solar cell efficiency because the photogenerated charges extract at the electrode depends on the competition between carrier sweep out, which is limited by the carrier mobility, and the loss of photogenerated carriers by recombination [40]. The hole and electron mobility of optimized **VC117**:PC$_{71}$BM BHJ active layer processed with/without pyridine additive and subsequent thermal annealing were estimated by space charge limited current (SCLC) method (J-V characteristics in dark) using the hole only device (ITO/PEDOT:PSS/ **VC117**:PC$_{71}$BM/Au) and the electron only device (ITO/Al/**VC117**:PC$_{71}$BM/Al), respectively. The results were analyzed using the SCLC model described by Mott-Gurney law which includes a small field dependent term, as seen in following equation [41].

$$J = \frac{9}{8}\varepsilon_r\varepsilon_o\mu_o\frac{(V_{app} - V_{bi})^2}{L^3}\exp\left(\beta\sqrt{\frac{V_{app} - V_{bi}}{L}}\right)$$

Where $\varepsilon_r\varepsilon_o$ is the dielectric permittivity of the active layer, L is the thickness of the active layer, V_{app} is the applied voltage, V_{bi} is the built in voltage, μ_o is the zero field mobility, and β is the field activation factor.

The J-V characteristics of the hole only device in dark were shown in Figure 10. The fitting of the experimental results (solid lines) revealed that the hole mobilities are found to be 6.21 x10^{-6} cm^2/Vs, 5.05 x10^{-5} cm^2/Vs and 8.45 x10^{-5} cm$^{2/}$Vs for the device without and with pyridine additives and subsequent thermally annealed, respectively. Although the thickness of the active layer influences the charge carrier mobility, and we taken much care to

ensure alike film thickness of the active layer (90 nm ±5 nm) and avoid substantial influence of this parameter on the devices charge mobility. The increase in the pyridine additives and thermally annealed agrees well with the results revealed by the morphology analysis, in which the domain size and crystallinity decreases and increases, respectively with the pyridine additives and subsequent thermally annealed. The electron mobility of the active layer processed without/with pyridine additive and thermally annealed are quite similar, i.e. 2.29×10^{-4} cm^2/Vs, 2.34×10^{-4} cm^2/Vs, and 2.38×10^{-4} cm^2/Vs respectively. The ratio of electron to hole mobilities in the active layer processed without/with additive and subsequent thermal annealing is found to be about 36, 4.63 and 2.81, respectively. Therefore it seems that in the active layer processed with pyridine and subsequent thermal annealing, the charge carrier transports are more balanced, a feature that increases the short circuit current, J_{sc} and the fill factor, FF, of the device, leading to a higher overall PCE value.

We have estimated the series resistance (R_s) and shunt resistance (R_{sh}) from the slope of the J-V characteristics of the devices, under illumination, around the V_{oc} and J_{sc}, respectively and complied in Table 3. In general, the R_s of the organic solar cell is composed of the bulk resistance of the active layer and depends on the charge transport ability within the active layer and morphology of the active layer. It can be seen from the table 1 that Rs of the device processed with pyridine/THF solvent is significantly lower than that for processed with THF and further decreased, that may be attributed to better morphology and balanced charge transport. Therefore, the higher boiling point of pyridine offers more time for the adjustment of molecular aggregation to improve the morphology and interpenetrating pathways network for charge transport, reducing the R_s and increasing the J_{sc} and FF [42]. The increase in R_{sh} is related to the decrease in leakage current and depends upon the intermolecular interaction (or electronic) coupling between the donor and acceptor materials in the active layer. Therefore, the slight decrease in the V_{oc} for the device processed with additive could be due to the increasing intermolecular interaction between the donor and acceptor.

We further studied the effect on the charge generation in the **VC117**:PC$_{71}$BM BHJ solar cells i.e. device A, B and C by investigating the saturation point where the internal field is large enough to sweep out all the carriers to the electrodes prior to recombination. Figure 6 shows the variation of photocurrent density (J_{ph}) with the internal voltage (V_{int}) of the device processed THF and pyridine/THF and pyridine/THF (solvent additive), under illumination at 100 mW/cm^2. J_{ph} is estimated as $J_{ph}=J_L-J_d$, where J_L and J_d are the current density under

illumination and in the dark, respectively [38a]. V_{int} is determined as $V_{int} = V_o - V$, where V_o is the voltage at which J_{ph} is zero and V is the applied voltage.[69,70] Therefore, V_{int} corresponds to the strength of electric field within the device needed to extract the charge carriers. As it can be seen from Figure 6, J_{ph} increases linearly with voltage at low V_{int}, but saturates at high V_{int} (1.8 V or higher). Therefore, we assume that almost all the photogenerated charge carriers within the device are collected at high V_{int} and J_{ph} saturated and independent of V_{int}. The J_{ph} at $V_{int} = 2.9$ V is found to be at about 15.03 mA/cm^2, 16.07 mA/cm^2 and 16.29 mA/cm2 for the device A, B and C, respectively, suggesting that the charge generation in the devices is influenced by the solvent additives. The charge collection probability (P_c) of the solar cells based on the active layers processed with THF, pyridine/THF and pyridine/THF (thermally annealed) was estimated as $P_c = J_{sc}/ J_{ph,sat}$, and were found to be about 0.56, 0.64 and 0.72 respectively. The low charge generation could be explained in terms of inefficient photon absorption and /or charge separation. Concerning the former parameter, the UV-visible absorption bands of **VC117**:PC$_{71}$BM BHJ active layer processed with pyridine additive are stronger than the corresponding processed without additive (see Figure 5) proving that there is indeed a difference in photon absorption. Nevertheless, the charge separation is another significant parameter that cannot be neglected, as there is a difference between the two devices in terms of domain size of the phase separation, as confirmed by TEM images, which is critical to charge recombination. So as the excitons are generated away from the D/A interfaces, they are not able to reach the interfaces in the large domain size of phase separation in the device processed in THF and the chances of recombination before the excitons are dissociated into free charge carriers, are increased. However, the solvent additive reduces this domain size and increases the D/A interfacial area so that more excitons are dissociated into free charge carriers.

Conclusions

In this report we presented the synthesis, optical and electrochemical properties of an A–π-D–π-A porphyrin small molecule in which ethyl rhodanine end capping groups were linked to core porphyrin donor via octyl thiophenes -ethynylene π-bridge i.e. VC117, as used as electron donor for the fabrication of solution processed BHJ solar cells, along with PC$_{71}$BM as electron acceptor. The optical and electrochemical properties of **VC117** suggest that **VC117:**PC$_{71}$BM blend can effectively harvest photons and transfer electrons from **VC117** to PC$_{71}$BM, resulting in a photovoltaic effect. The solar cell based on a **VC117**:PC$_{71}$BM BHJ active layer with optimized 1:1 weight ratio, processed from THF,

displayed a PCE value of 2.95 %. In order to improve the efficiency of this organic solar cell, the **VC117**:PC$_{71}$BM BHJ active layer was processed from a solvent mixture of 4% v/v of pyridine in THF and subsequent thermal annealing. The PCE value of the resulting devices B and C was improved up to 4.46 % and 5.50 %, respectively, as a result of the enhancement of its J$_{sc}$ and FF values, parameters that are related to the charge generation / separation /mobility/transport that are found to be significantly improved by the morphology and crystallinity change of the active layer upon addition of pyridine and further improved with thermal annealing.

Acknowledgements

References

1. (a) F. C. Krebs, N. Espinosa, M. Ho ¨sel, R. R. Søndergaard and M. Jørgensen, *Adv. Mater.,* 2014, **26**, 29; (b) W. Li, W. S. C. Roelofs, M. Turbiez, M. M. Wienk and R. A. J. Janssen, *Adv. Mater*., 2014, **26**, 3304; (c) L. Bian, E. Zhu, J. Tang, W. Tang and F. Zhang, *Prog. Polym. Sci*., 2012, **37**, 1292; (d) S. H. Liao, H. J. Jhuo, P. N. Yeh, Y. S. Cheng, Y. L. Li, Y. H. Lee, S. Sharma and S. A. Chen, *Sci. Rep*., 2014, **4**, 6813; (e) A. J. Heeger, Adv. Mater., 2014, 26, 10; (f) X. Guo, M. Baumgarten and K. Müllen, *Prog. Polym. Sci*., 2013, **38**, 1832.

2. (a) Y. Liu, J. Zhao, Z. Li, C. Mu, W. Ma, H. Hu, K. Jiang, H. Lin, H. Ade and H. Yan, *Nat. Commun*., 2014, **5**, 5293; (b) C. C. Chen, W. H. Chang, K. Yoshimura, K. Ohya, J. You, J. Gao, Z. Hong and Y. Yang, *Adv. Mater*., 2014, **26**, 5670; (c) C. Z. Li, C. Y. Chang, Y. Zang, H. X. Ju, C. C. Chueh, P. W. Liang, N. Cho, D. S. Ginger and A. K.-Y. Jen, *Adv. Mater*., 2014, **26**, 6262; (d) H. Kang, S. Kee, K. Yu, J. Lee, G. Kim, J. Kim, J. R. Kim, J. Kong and K. Lee, *Adv. Mater*., 2015, **27**, 1408.

3. J. You, L. Dou, K. Yoshimura, T. Kato, K. Ohya, T. Moriarty, K. Emery, C.-C. Chen, J. Gao, G. Li and Y. Yang, *Nat. Commun*., 2013, **4**, 1446

4. (a) P. M. Beaujuge and J. M. J. Fréchet, *J. Am. Chem. Soc*. 2011, **133**, 20009, (b) Y. Li, *Acc. Chem. Res*. 2012, **45**, 723; (b) H. Zhou, L. Yang and W. You, *Macromolecules* 2012, **45**, 607; (c) C. Z. Li, C.Y. Chang, Y. Zang, H.X. Ju, C. C. Chueh, P.W. Liang, N. Cho, D. S. Ginger and A. K. Jen, *Adv. Mater*., 2014, **26**, 6262; (d) L. Lu and L. Yu, *Adv. Mater.*, 2014, **26**, 4413

5. (a) Y. J. He, H. Y. Chen, J. H. Hou and Y. F. Li, *J. Am. Chem. Soc*., 2010, **132**, 1377; (b) A. Eftaiha, J. Sun, I. Hill and G. Welch, *J. Mater. Chem. A* 2014, **2**, 1201.

6. (a) C. He, S. Su, M. Xu, H. Wu and Y. Cao, *Nat. Photon*. 2012, **6**, 591; (b) L. Dou, J. You, Z. Hong, Z. Xu, G. Li, R. A. Street and Y. Yang, *Adv. Mater*., 2013, **25**, 6642; (c) C. Duan, K. Zhang, C. Zhong, F. Huang and Y. Cao, *Chem. Soc. Rev*., 2013, **42**, 9071; (d) J. Kong, I. W. Hwang and K. Lee, *Adv. Mater*., 2014, **26**, 6275; (e) M.T. Dang and J. D. Wuest, *Chem. Soc. Rev*., 2013, **42**, 9105; (e) T. Ameri, N. Li and C.J. Brabec, *Energy Environ. Sci*., 2013, **6**, 2390; (f) J. Mei and Z. Bao, *Chem. Mater*., 2014, **26**, 604; (g) L. Ye, S. Zhang, L. Huo, M. Zhang and J. Hou, *Acc. Chem. Res*. 2014, **47**, 1595.

7. H. J. Song, D. H. Kim, E. J. Lee and D. K. Moon, *J. Mater. Chem. A* 2013 **1** 6010-6020.

8. (a) B. Walker, C. Kim and T. Q. Nguyen, *Chem. Mater*., 2011, **23**, 470; (b) J. Roncali, P. Leriche and P. Blanchard, *Adv. Mater*., 2014, **26**, 3821; (c) A. Mishra and P. Bä uerle, *Angew. Chem., Int. Ed*. 2012, **51**, 2020; (d) Y. Lin, Y. Li and X. Zhan*, Chem. Soc. Rev*., 2012, **41**, 4245; (e) Y. Sun, G. Welch, W. Leong, C. Takacs, G. C. Bazan, and A. J. Heeger, *Nat. Mater*., 2012, **11**, 44; (f) J. E. Coughlin, Z. B. Henson, G. C. Welch and G. C. Bazan. Acc. Chem. Res., 2014, **47**, 257.

9. (a) A. K. K. Kyaw, D. H. Wang, D. Wynands, J. Zhang, T. Q. Nguyen, G. C. Bazan and A. J. Heeger, *Nano Lett*., 2013, **13**, 3796; (b) J. Zhou, Y. Zuo, X. Wan, G. Long, Q. Zhang, W. Ni, Y. Liu, Z. Li, G. He, C. Li, B. Kan, M. Li and Y. Chen, *J. Am. Chem. Soc.,* 2013, **135**, 8484; (c) Q. Zhang, B. Kan, F. Liu ,G. Long, X. Wan, X. Chen,Y. Zuo, W. Ni, H. Zhang, M. Li, Z. Hu, F. Huang, Y. Cao, Z. Liang, M. Zhang, T. P. Russell and Y. Chen, Nat. Photonics doi: 10.1038/NPHOTON.2014.269; (d) V. Gupta, A. K. K. Kyaw, D. H. Wang, S. Chand, G. C. Bazan and A. J. Heeger, Sci. Rep. 3 : 1965, DOI: 10.1038/srep01965; (e) Y. Liu, C. C. Chen, Z. Hong, J. Gao, Y. (Michael) Yang, H. Zhou, L. Dou, G. Li and Y. Yang, Sci. Rep 3:3356 doi: 10.1038/srep03356; (f) B. Kan, Q. Zhang, M. Li, X. Wan, W. Ni, G. Long, Y. Wang, X. Yang, H. Feng, and Y. Chen, *J. Am. Chem. Soc.* doi: 10.1021/ja509703k; (g) B. Kan, M. Li, Q. Zhang, F. Liu, X. Wan, Y. Wang, W. Ni, G. Long, X. Yang, H. Feng, Y. Zuo, M. Zhang, F. Huang, Y. Cao, T. P. Russell and Y. Chen, *J. Am. Chem. Soc*., 2015, **137**, 3886.

10. (a) C. W. Tang and A. C. Albrecht, *Nature* 1975, **254**, 507; (b) A. Goetzberger, C. Hebling and H. W. Schock, *Mater. Sci. Eng*., 2003, **R40**, 1; (c) L. L. Li and E. W.-G. Diau, *Chem. Soc. Rev*., 2013, **42**, 291.

11. (a) T. Umeyama, T. Takamatsu, N. Tezuka, Y. Matano, Y. Araki, T. Wada, O. Yoshikawa, T. Sagawa, S. Yoshikawa and H. Imahori, *J. Phys. Chem. C* 2009, **113**, 10798; (b) S. J. Lee, K. L. Mulfort, X. Zuo, A. J. Goshe, P. J. Wesson, S. T. Nguyen, J. T. Hupp and D. M. Tiede, *J. Am. Chem. Soc*., 2008, **130**, 836−838; (c) M. S. Kang, J. B. Oh, K. D. Seo, H. K. Kim, J. Park, K. Kim and N. G. Park, *J. Porphyrins Phthalocyanines*, 2009, **13**, 798; (d) H. Imahori, T. Umeyama and S. Ito, *Acc. Chem. Res*., 2009, 42, 1809; (e) R. B. Ambre, G.-F. Chang, M. R. Zanwar, C.-F. Yao, E. W.-G. Diau and C.-H. Hung, *Chem. Asian J*., 2013, 8, 2144–2153.

12. (a) M. Urbani and Michael Grä tzel, M. K. Nazeeruddin, T. Torres, *Chem. Rev*., doi: 10.1021/cr5001964; (b) T. Higashino and H. Imahori, *Dalton Trans*. doi: 10.1039/c4dt02756f, (c) M. K. Panda, K. Ladomenou, A. G. Coutsolelos, *Coord.*

Chem. Rev., 2012, **256**, 2601–2627, (d) K. Ladomenou, T. N. Kitsopoulos, G. D. Sharma and A. G. Coutsolelos, *RSC Adv*., 2014, **4**, 21379

13. (a) S. Mathew, A. Yella, P. Gao, R. Humphry-Baker, B. F. E.Curchod, N. Ashari-Astani, I. Tavernelli, U. Rothlisberger, M. K. Nazeeruddin and M. Gra¨tzel, *Nat. Chem*., 10.1038/NCHEM.1861 (b) A. Yella, H.-W. Lee, H. N. Tsao, C. Yi, A. K. Chiran, M. K. Nazeeruddin, E. W.-G. Diau, C.-Y. Yeh, S. M. Zakeeruddin and M. Gratzel, *Science* 2011, **334**, 629.

14. (a) J. Hatano, N. Obata, S. Yamaguchi, T. Yasuda and Y. Matsuo, *J. Mater. Chem*., 2012, 22, 19258, (b) T. Yamamoto, J. Hatano, T. Nakagawa, S. Yamaguchi, and Y. Matsuo, *Appl. Phys. Lett*., 2013, **102**, 013305, (c) T. Nakagawa, J. Hatano and Y. Matsuo, *J. Porphrin Phthalocyanines* 2014, **18**, 735-740, (d) Y. Matsuo, J. Hatano and T. Nakagawa, *J. Phys. Org.Chem*., 2014, **27**, 87-93, (e) T. Sato, T. Nakagawa, H. Okada and Y. Matsuo, *J. Porphyrins and Phthalocyanines*, 2015, **19**, 451-458

15. (a) Y. Huang, L. Li, X. Peng, J. Peng and Y. Cao, *J. Mater. Chem*., 2012, **22**, 21841, (b) L. Li, Y. Huang, J. Peng, Y. Cao and X. Peng, *J. Mater. Chem. A*, 2013, **1**, 2144, (c) G. D. Sharma, D. Daphnomili, S. Biswas and A. G. Coutsolelos, Org. Electron., 2013, 14, 1811, (d) G. D. Sharma, G. E. Zervaki, P. A. Angaridis, T. N. Kitsopoulos and A. G. Coutsolelos, *J. Phys. Chem. C* 2014, **118**, 5968; (e) J. Kesters, P. Verstappen, M. Kelchtermans, L. Lutsen, D. Vanderzande and W. Maes, *Adv. Energy Mater.* doi: 10.1002/aenm.201500218

16. (a) H. Qin, L. Li, F. Guo, S. Su, J. Peng, Y. Cao and X. Peng, *Energy Environ. Sci*., 2014, **7**, 1397, (b) K. Gao, L. Li, T. Lai, L. Xiao, Y. Huang, F. Huang, J. Peng, Y. Cao, F. Liu, T. P. Russell, R. A. J. Janssen and X. Peng, J. Am. Chem. Soc. doi:10.1021/jacs.5b03740

17. (a) Y. Liu, X. Wan, B. Yin, J. Zhou, G. Long, S. Yin and Y. Chen, J. Mater. Chem. 2010, **20**, 2464; (b) K. Schulze, C. Uhrich, R. Schuppel, K. Leo, M. Pfeiffer, E. Brier, E. Reinold, and P. Bauerle, *Adv. Mater.,* 2006, **18**, 2872.

18. (a) Y. S. Liu, X. Wan, F. Wang, J. Zhou, G. Long, J. Tian and Y. Chen, *Adv. Mater.*, 2011, **23,** 5387; (b) Y. S. Liu, X. Wan, F. Wang, J. Zhou, G. Long, J. Tian, J. You, Y. Yang, and Y. Chen,*Adv. Energy. Mater*., 2011, **1**, 771; (c) J. Y. Zhou, X. Wan, Y. Liu, G. Long, F. Wang, Z. Li, Y. Zuo, C. Li and Y. Chen, *Chem. Mater.,* 2011, **23**, 4666; (d) Y. S. Liu, Y. Yang, C.C. Chen, Q. Chen, L. Dou, Z. Hong, G. Li and Y. Yang, *Adv. Mater.*, 2013, **25**, 4657.

19. (a) Z. Li, G. He, X. Wan, Y. Liu, J. Zhou, G. Long, Y. Zuo, M. Zhang and Y. Chen, *Adv. Energy. Mater*., 2012, **2**, 74; (b) J. Y. Zhou, X. Wan, Y. Liu, Y. Zuo, Z. Li, G. He, G. Long, W. Ni, C. Li, X. Su and Y. Chen, *J. Am. Chem. Soc*. 2012, **134**, 16345; (c) J. Y. Zhou, Y. Zuo, X. Wan, G. Long, Q. Zhang, W. Ni, Y. Liu, Z. Li, G. He, C. Li, B. Kan, M. Li and Y. Chen, *J. Am. Chem. Soc.,* 2013, **135**, 8484

20. Challuri Vijay Kumar, L. Cabau, E. N. Koukaras, G. D. Sharma and E. Palomares, *Nanoscale* 2015, **7**, 179.

21. J. Zhou, X. Wan, Y. Liu, G. Long, F. Wang, Z. Li, Y. Zuo, C. Li, Y. Chen, *Chem. Mater.*, 2011, **23**, 4666−4668.

22. T. R. Sanchis, B. C. Guo, H. P. Wu, T. Y. Pan, H. W. Lee, S. R. Raga, F. Fabreqat-Santiago, J. Bisquert, C.Y. Yeh, and E.W. G. Diau, *Chem. Commun.,* 2012, **48,** 4368.

23. T. E. O. Screen, K. B. Lawton, G. S. Wilson, N. Dolney, R. Ispasoiu, T. Goodson III, S. J. Martin, D. D. C. Bradley and H. L. Anderson, *J. Mater. Chem.*, 2001, **11**, 312.

24. (a) V. S.-Y. Lin, S. G. DiMagno and M. J. Therien, Science, 1994, 264, 1105; (b) C. Y. Lee, C. She, N. C. Jeong and J. T. Hupp, Chem. Commun., 2010, 46, 6090

25. J. P. Perdew, K. Burke and M. Ernzerhof, *Phys. Rev. Lett.* 1996, **77**, 3865.

26. A. Schafer, H. Horn and R. Ahlrichs, *J. Chem. Phys.* 1992, **97**, 2571.

27. K. Eichkorn, O. Treutler, H. Öhm, M. Häser and R. Ahlrichs, *Chem. Phys. Lett.* 1995, **240**, 283.

28. (a) A. D. Becke, *J. Chem. Phys.* 1993, **98**, 5648; (b) C. Lee, W. Yang and R. G. Parr, *Phys. Rev. B* 1988, **37**, 785.

29. Y. Zhao and D. G. Truhlar, *Theor. Chem. Acc.* 2008, **120**, 215.

30. Frisch, M. J.; Trucks, G. W.; Schlegel, H. B.; Scuseria, G. E.; Robb, M. A.; Cheeseman, J. R.; Scalmani, G.; Barone, V.; Mennucci, B.; Petersson, G. A.; Nakatsuji, H.; Caricato, M.; Li, X.; Hratchian, H. P.; Izmaylov, A. F.; Bloino, J.; Zheng, G.; Sonnenberg, J. L.; Hada, M.; Ehara, M.; Toyota, K.; Fukuda, R.; Hasegawa, J.; Ishida, M.; Nakajima, T.; Honda, Y.; Kitao, O.; Nakai, H.; Vreven, T.; Montgomery, Jr., J. A.; Peralta, J. E.; Ogliaro, F.; Bearpark, M.; Heyd, J. J.; Brothers, E.; Kudin, K. N.; Staroverov, V. N.; Kobayashi, R.; Normand, J.; Raghavachari, K.; Rendell, A.; Burant, J. C.; Iyengar, S. S.; Tomasi, J.; Cossi, M.; Rega, N.; Millam, J. M.; Klene, M.; Knox, J. E.; Cross, J. B.; Bakken, V.; Adamo, C.; Jaramillo, J.; Gomperts, R.; Stratmann, R. E.; Yazyev, O.; Austin, A. J.; Cammi, R.; Pomelli, C.; Ochterski, J. W.; Martin, R. L.; Morokuma, K.; Zakrzewski, V. G.; Voth, G. A.; Salvador, P.; Dannenberg, J. J.; Dapprich, S.; Daniels, A. D.; Farkas, Ö.; Foresman, J. B.; Ortiz, J. V.; Cioslowski, J.; Fox, D. J. Gaussian 03, revision C.01; Gaussian, Inc.: Wallingford CT, 2004.

31. TURBOMOLE (version 5.6); Universitat Karlsruhe, 2000.

32. D. Jacquemin, E. A. Perpète, I. Ciofini, Adamo; R. Valero, Y. Zhao and D. G. Truhlar, *J. Chem. Theory Comput.* **2010**, 6, 2071–2085.

33. S.R. Cowan, W. L. Leong, N. Banerji, G. Dennler, A. J. Hegger, *Adv. Funct. Mater.* **2011**, 21, 3083-3092

34. Y. Li, *Acc. Chem. Res.* 2012, **45**, 723.

35. (a) W. Ma, C. Yang, X. Gong, K. Lee and A. J. Heeger, *Adv. Funct. Mater.,* **2005**, **15**, 1617; (b) J. A. Mikroyannidis, A. N. Kabanakis, S. S. Sharma and G. D. Sharma, *Adv. Funct. Mater.,* 2011, **21**, 746.

36. (a) J. E. Coughlin, Z. B. Henson, G. C. Welch, G. C. Bazan, *Acc. Chem. Res.* 2013, **47**, 257; (b) Y. Chen, X. Wan and G. Long, *Acc. Chem. Res.* 2013, **46**, 2645.

37. (a) J. Peet, J. Y. Kim, N. E. Coates, W. L.Ma, D. Moses, A. J. Heeger, G. C. Bazan, *Nat. Mater.,* 2007, *6*, 497; (b) M. S. Su, C. Y. Kuo, M. C. Yuan, U. S. Jeng, C. J. Su and K. H. Wei, *Adv. Mater.,* 2011, **23**, 3315; (c) A. Tamayo, T. Kent, M. Tantitiwat, M. A. Dante, J. Rogers and T. Q. Nguyen, *Energy Environ. Sci.,* 2009, **2**, 1180; (d) H. Fan, H. Shang, Y. Li and X, Zhan, *Appl. Phys. Lett.,* 2010, **97**, 133302; (e) B. Walker, C. Kim and T. Q. Nguyen, *Chem. Mater.,* 2011, **23**, 470.

38. M. C. Yuan, M. Y. Chiu, S. P. Liu, C. M. Chen and K. H. Wei, *Macromolecules* 2010, **43**, 6936.

39. B. Qi and J. Wang, *Phys. Chem. Chem. Phys.* 2013, **15**, 8972.

40. (a) S. R. Cowan, A. Roy and A. J. Heeger, *Phys. Rev. B* 2010, **82**, 245207; (b) a. K. K. Kyaw, D. H. Wang, C. Luo, Y. Cao, T. Q. Nguyen, G. C. Bazan and A. J. Heeger, *Adv. Energy Mater.,* 2014, **4**, 1301469.

41. (a) P. N. Murgatroyd, *J. Phys. D: Appl. Phys.,* 1970, **3**, 151; (b) V. D. Mihailetchi, H. X. Xie, B. de Boer, L. J. A. Koster and P. W. M. Blom, *Adv. Funct. Mater.,* 2006, **16**, 699.

42. J. Huang, C. Zhan, X. Zhang, Y. Zhao, Z. Lu, H. Jai, B. Jiang, J. Ye, S. Zhang, A. Tang, Y. Liu, Q. Pei and J. Jao, *ACS Appl. Mater. Interface* 2013, **5**, 2030.

Table 1 Absorption, emission and electrochemical properties **VC117**

Material	λ_{abs} (nm)[a]	λ_{em} (nm)[a]	λ_{abs} (nm)[b]	$E_{g(opt)}$ (eV)[f]	E_{ox} (V vs Fc/Fc+)	E_{o-o} (eV)[c]	E_{HOMO} (ev)[d]	E_{LUMO} (ev)[e]
VC117	467 (229) 682 (73)	716	462, 694	1.62	0.25	1.77	-5.13	-3.36

[a]Measured in THF. In parenthesis molar extinction efficient at λ_{abs}(in $10^3 M^{-1}$ cm^{-1}), [b]measured in thin film cast from THF solution, [c]E_{0-0} was determined from the intersection of

absorption and emission spectra in dilute solutions. [d]$E_{HOMO}$was calculated using E_{HOMO}(vs vacuum) = -4.88-E_{ox}(vs Fc/Fc+). [e]E_{LUMO} was calculated using $E_{LUMO} = E_{HOMO} + E_{0-0}$, [f]calculated from onset absorption edge in the absorption spectra in thin film

Table 2 Calculated properties of **VC117**. Specifically HOMO and LUMO energies (eV), HOMO–LUMO gap (eV), *HL*, Optical gap (eV), *OG*, with corresponding oscillator strengths, *f*, the wavelengths of the first excitation and excitations with the largest oscillator strengths, the main contributions to the first excited state, and the dipole moment (D), μ.

	HOMO (eV)	LUMO (eV)	HL (eV)	OG (eV)	$\lambda_{1st/max}$ (nm)	f	Main Contributions	μ (D)
PBE	−4.42 −4.52[a]	−3.40 −3.53[a]	1.02 0.99[a]	1.17 1.11[a]	1062 1113[a]	1.69 2.31[a]	H→L (85%),H→L+2 (13%); H→L (91%),H→L+2 (8%)[a]	2.85
B3LYP	−4.86 −4.97[a]	−2.91 −3.05[a]	1.95 1.92[a]	1.71 1.63[a]	727/509/440/399 760/526/463/443/403[a]	2.89 2.88[a]	H→L (94%); H→L (94%)[a]	3.30 4.24[a]
M06	−5.12 −5.26[a]	−2.85 −3.01[a]	2.27 2.25[a]	1.78 1.71[a]	696/488/430/419/404/369 724/556/497/465/430/408/380[a]	2.88 3.09[a]	H→L (86%),H−1→L+3(5%), H→L+2 (4%); H→L (89%),H−2→L+3(4%)[a]	3.39 4.32[a]

[a] Values when solvent effects are taken into account for tetrahydrofuran.

Table 3 Photovoltaic parameters of organic solar cells based on **VC117**:PC$_{71}$BM active layer processed in different conditions

Solvent	J_{sc} (mA/cm^2)	V_{oc} (V)	FF	PCE (%)	R_s (Ohm)	R_{sh} (Ohm cm2)	μ (cm^2/Vs)
THF (device A)	8.38	0.82	0.43	2.95	54	213	6.21 x10^{-6}
Pyridine/THF (device B)	10.22	0.78	0.56	4.46	31	256	5.05x10^{-5}
Pyridine/THF[a] (device C)	11.67	0.76	0.62	5.50	18	324	8.45x10^{-5}

[a] thermal annealing
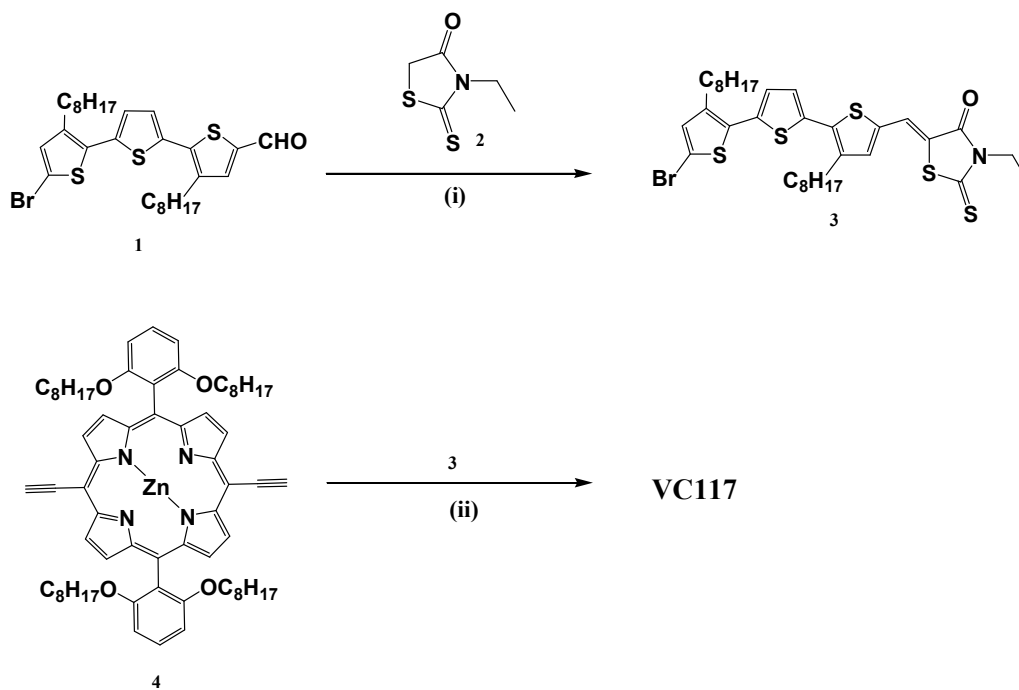
Scheme 1 Synthetic route of **VC117**. (*Reaction conditions):* (i) Dry Chloroform, Pipperdine Reflux,12h (ii) Pd$_2$(dba)$_3$,AsPh$_3$, dry THF ,NEt$_3$, reflux 12 h.
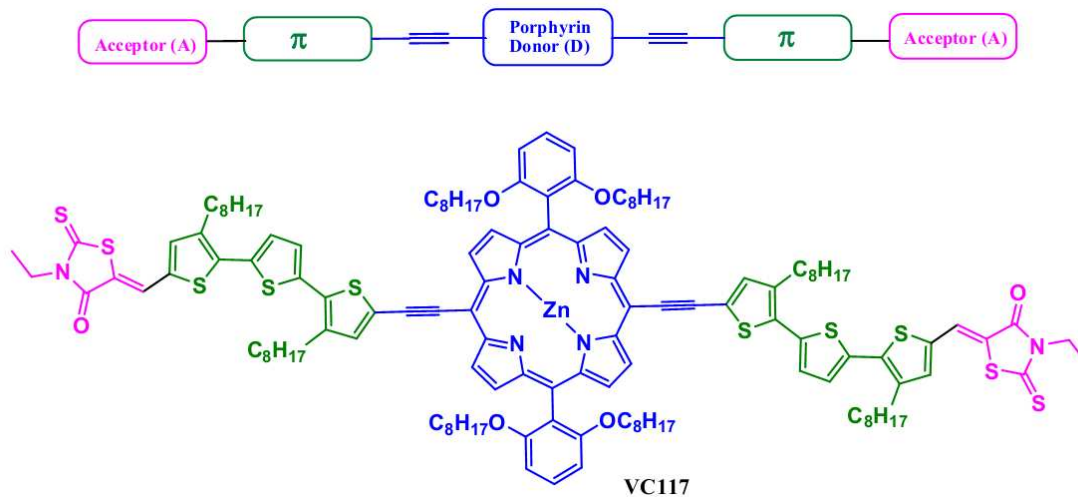
Scheme 2 General architecture of the A–π-D–π-A small molecule and the molecular structure of **VC117**
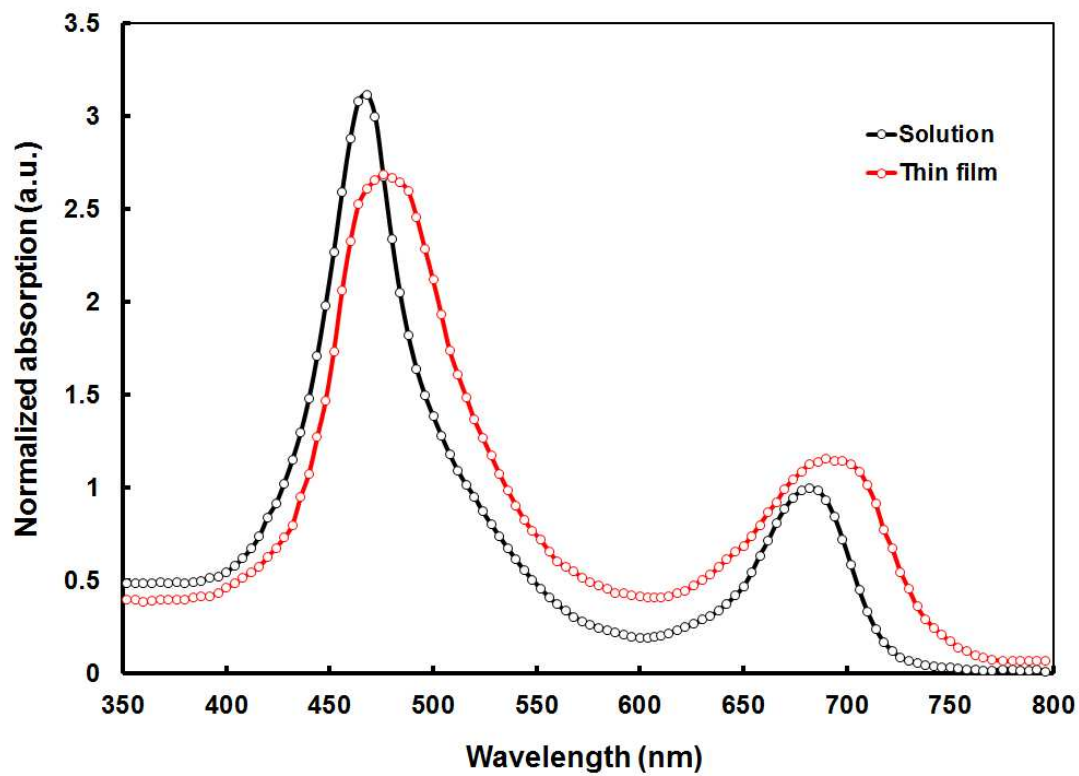
Figure 1 Normalized absorption spectra of **VC117** in THF solution and thin film cast from the THF solution.
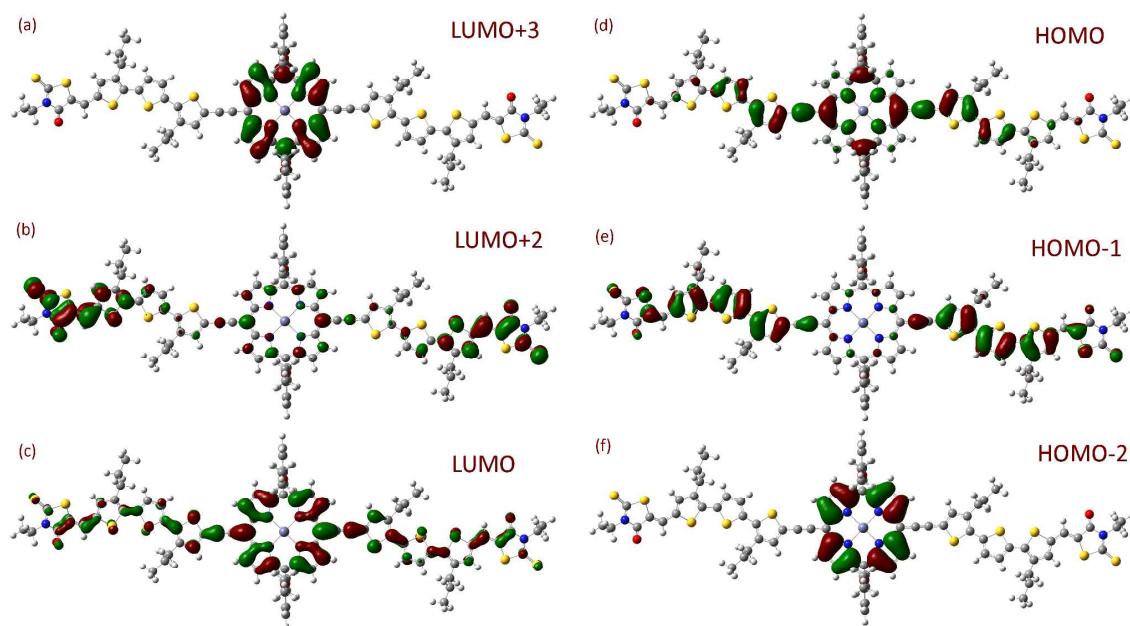
Figure 2 Frontier and near frontier orbitals of **VC117,** involved in transitions that contribute to the first excitation (alkyl groups have been shortened)
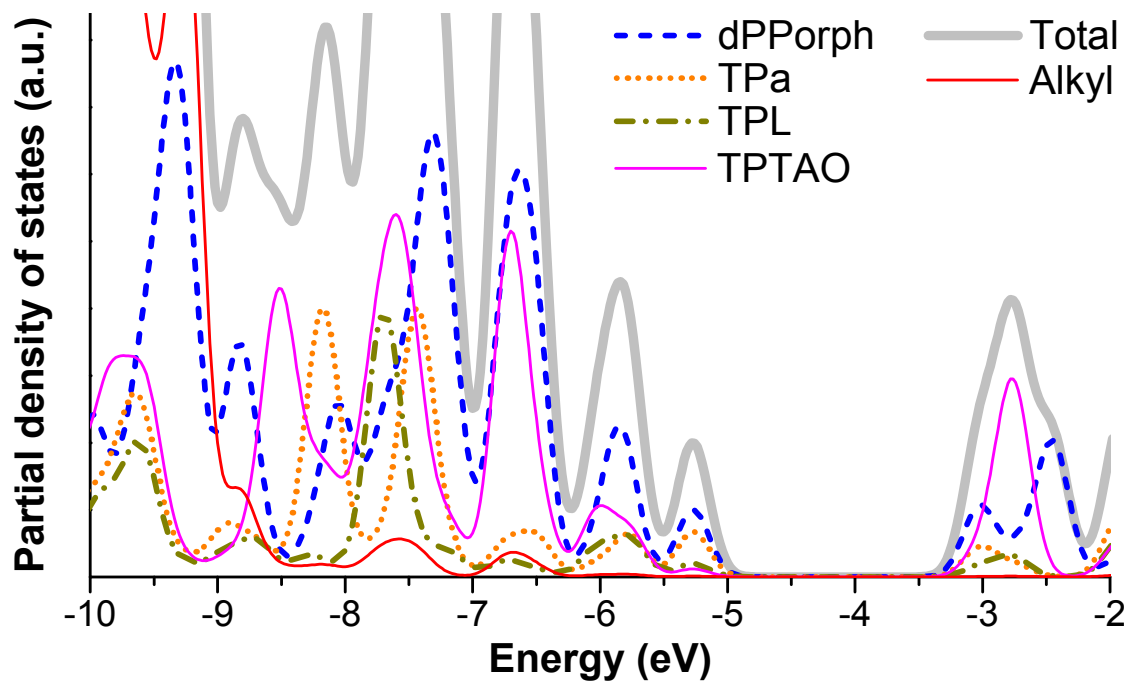
Figure 3 Total and partial density of states of **VC117** (calculated using the M06 functional)
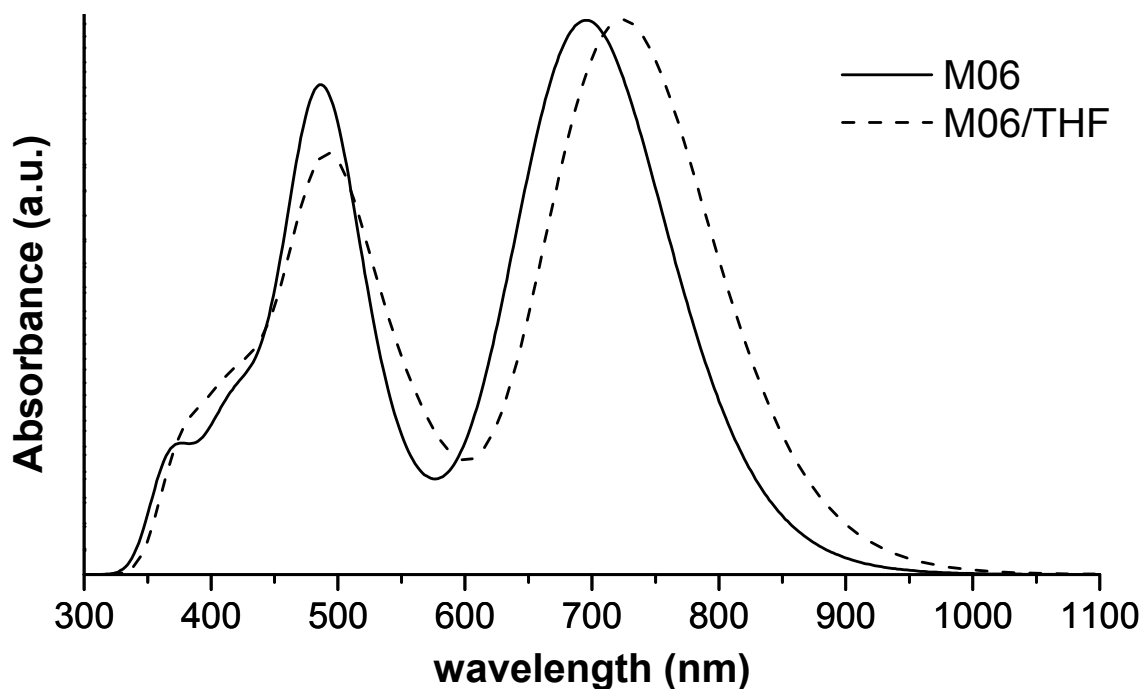
Figure 4 Theoretical UV/Vis absorption spectrum of **VC117** (calculated using the M06 functional).
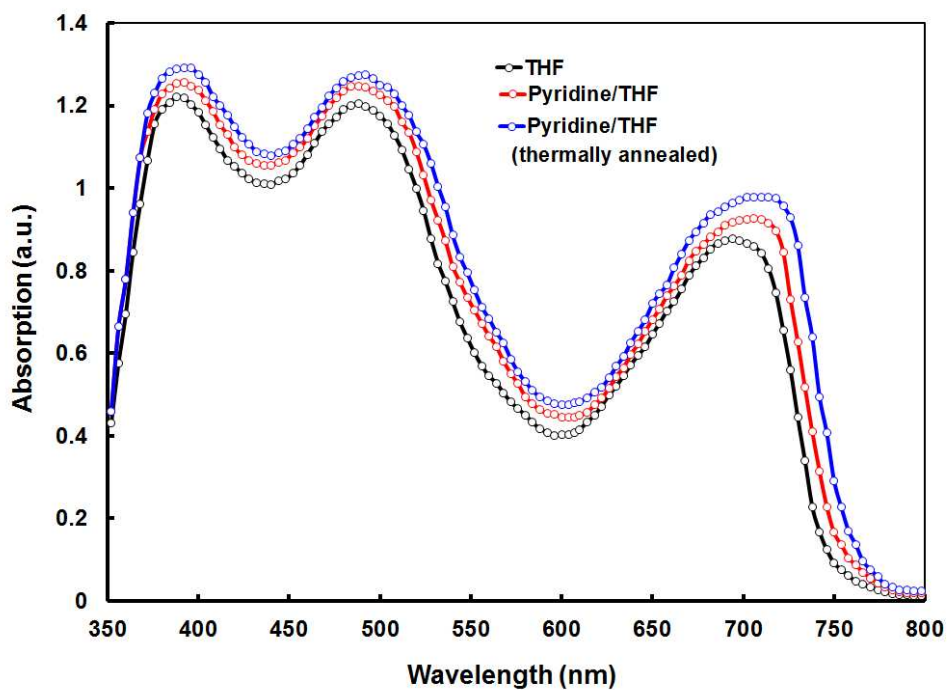
Figure 5 Normalized absorption spectra of **VC117**:PC$_{71}$BM (1:1) thin film processed under different conditions.
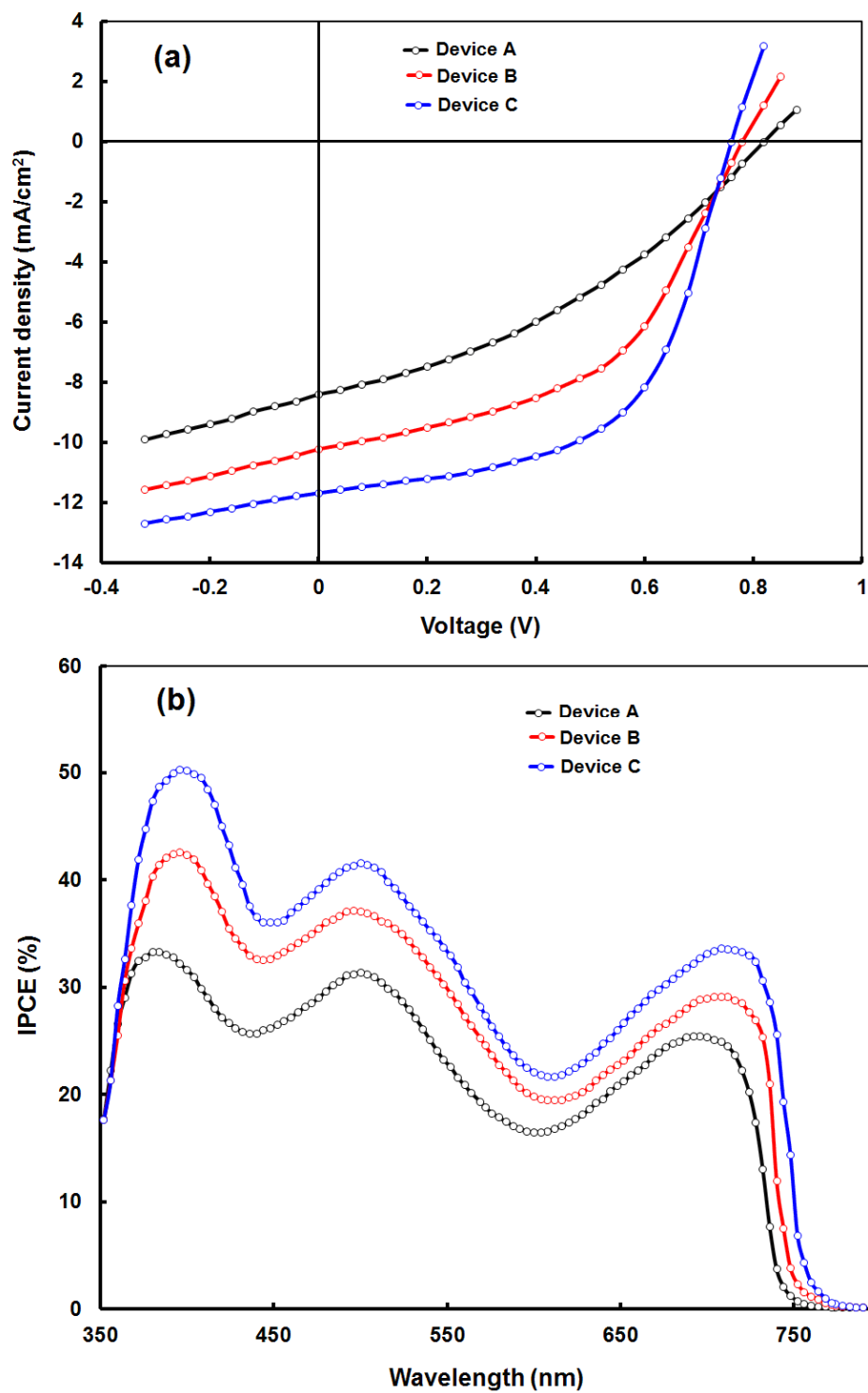
Figure 6 (a) Current-voltage characteristics under illumination and IPCE spectra of BHJ organic solar cells based on **VC117**:PC$_{71}$BM blends processed with different conditions.
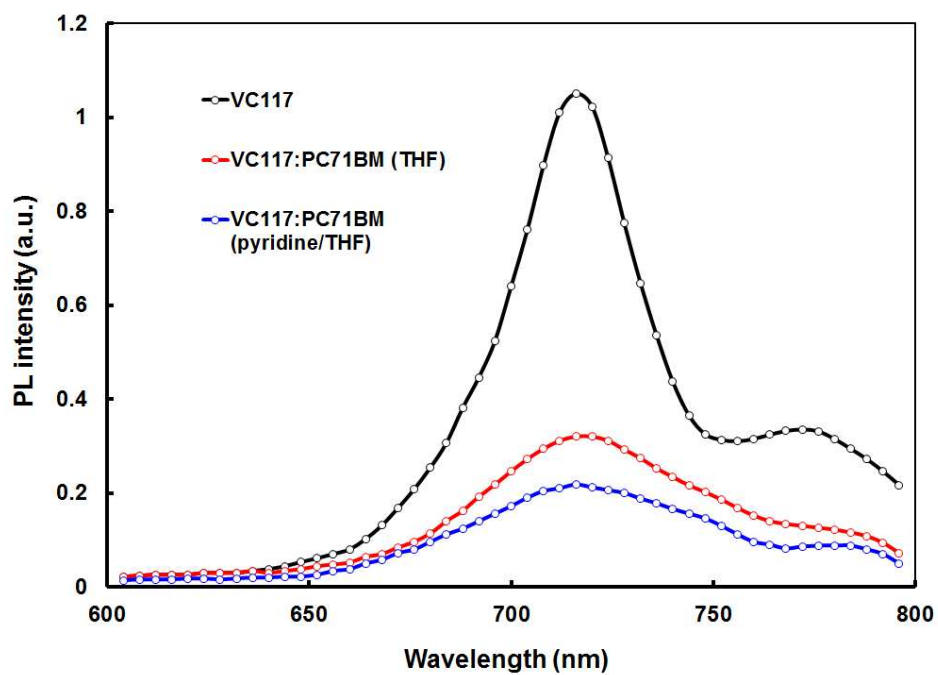
Figure 7 PL spectra of **VC117**, **VC117**:PC$_{71}$BM (THF) and **VC117**:PC$_{71}$BM (pyridine/THF) thin films
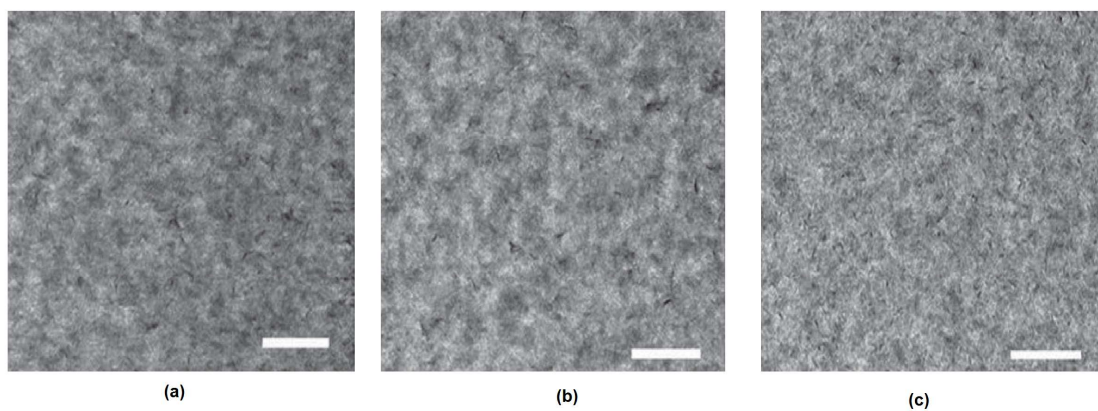
Figure 8 TEM morphology of thin films prepared with (a) THF (b) pyridine/THF, (c) pyridine/THF (thermal annealed). The scale bar is 300 nm
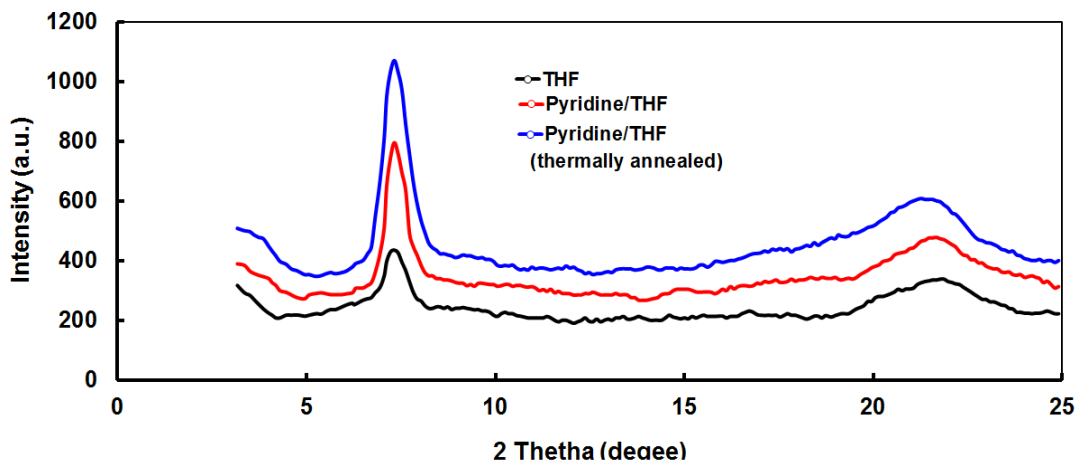
Figure 9 XRD patterns of the **VC117**:PC$_{71}$BM films processed THF, pyridine/THF and pyridine/THF (thermal annealed) under different conditions
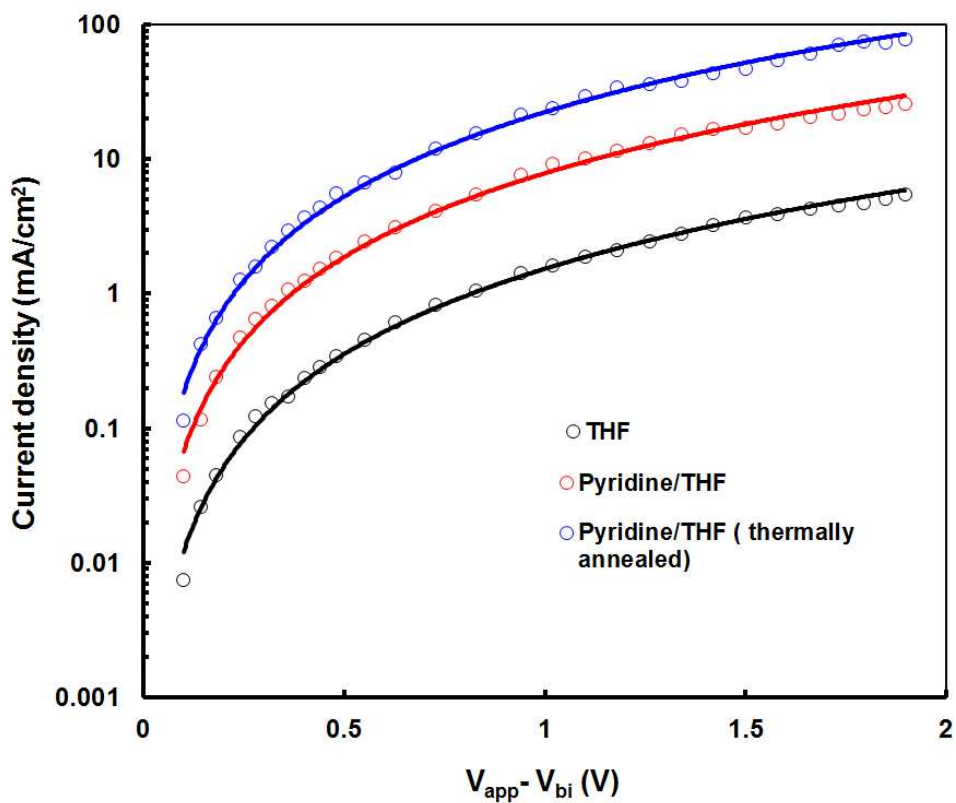
Figure 10 Current –voltage characteristics of hole only devices in dark based on **VC117**:PC$_{71}$BM blends processed in different conditions, to measure the hole mobility.
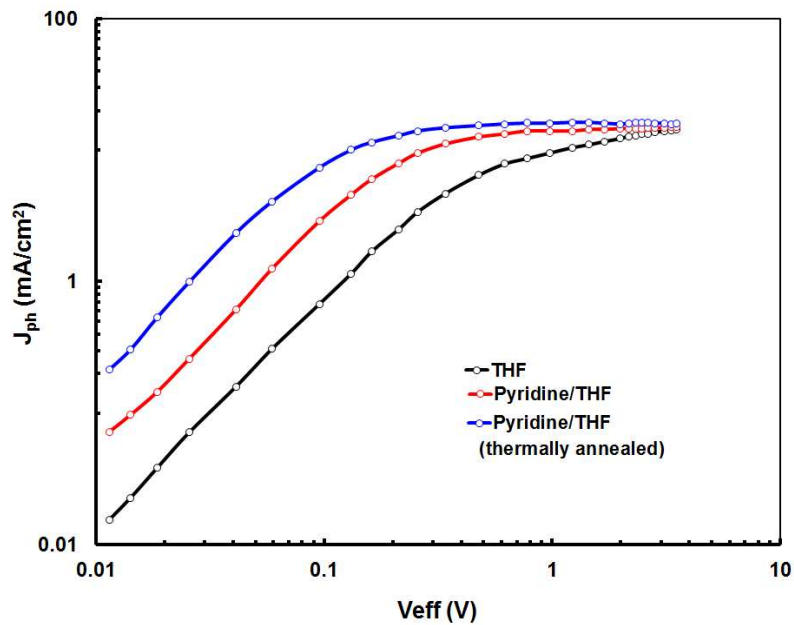
Figure 11 Photocurrent density (J_{ph}) variation with internal voltages (V_{in}) for **VC117**:$PC_{71}BM$ devices processed in different conditions.

TOC
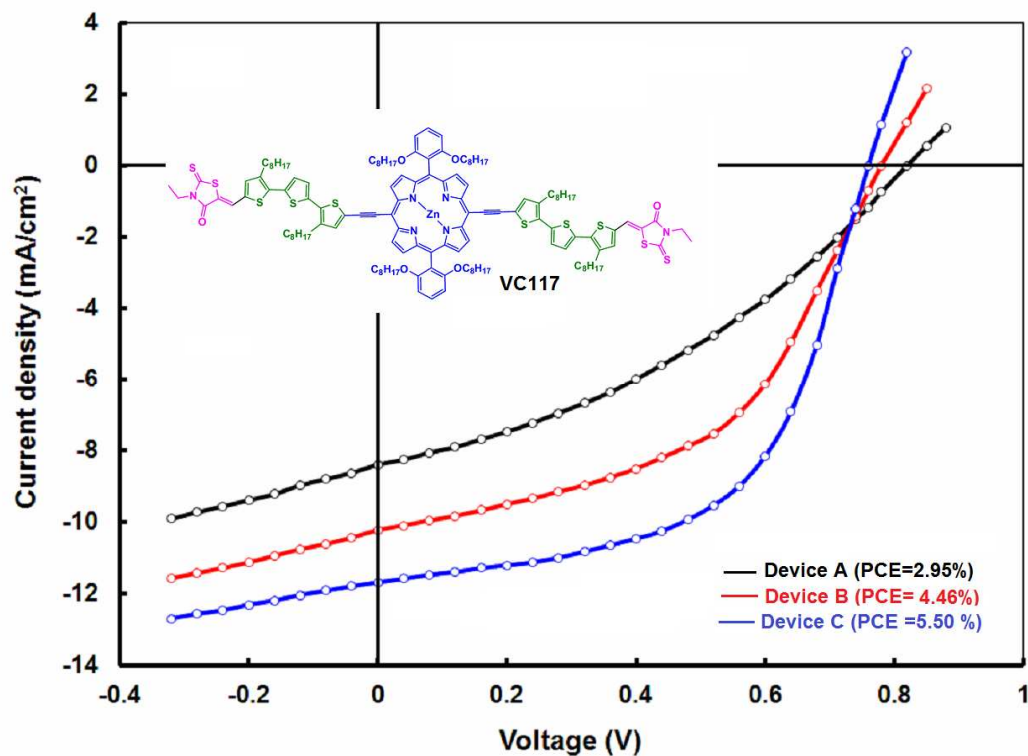
Device A **VC117**:PC$_{71}$BM (THF cast), device B **VC117**:PC$_{71}$BM (Pyridine/THF) and device C **VC117**:PC$_{71}$BM (Pyridine/THF) with thermal annealing